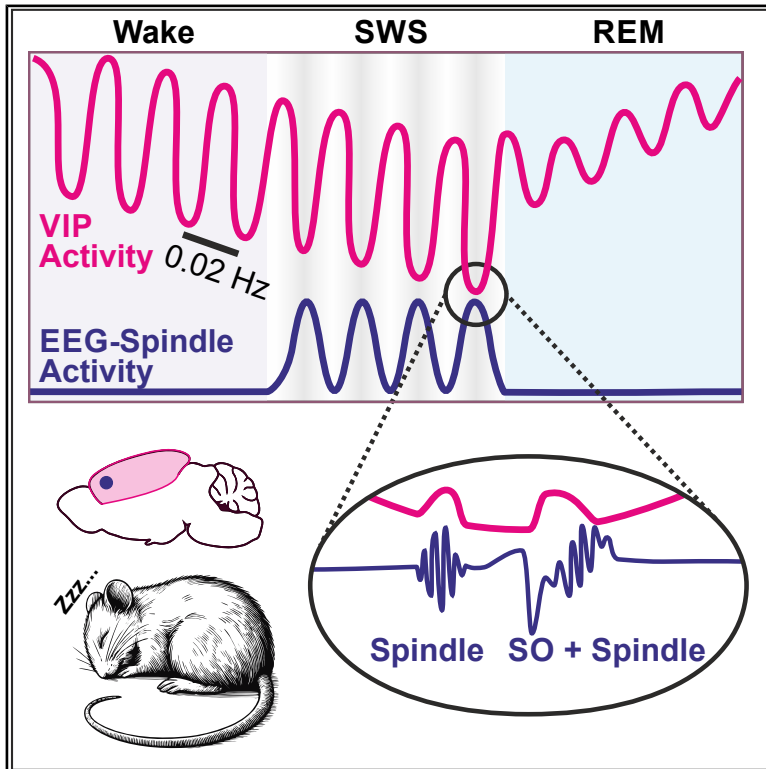


# VIP interneuron activity during sleep conveys the cortical infraslow oscillation

## Graphical abstract



## Authors

Kilian Rolle, Louisa Weber, Jan Born, Niels Niethard

## Correspondence

niels.niethard@uni-tuebingen.de

## In brief

Sleep promotes memory by reorganizing cortical circuits. Rolle et al. discovered that VIP interneurons, which regulate inhibition, are suppressed during slow-wave sleep but activated during spindles and slow oscillations. Their unique infraslow coupling to spindles, absent in SST and PV interneurons, suggests a specialized role in memory consolidation.

## Highlights

- VIP interneuron activity follows a 0.02-Hz infraslow rhythm during sleep and wakefulness
- The infraslow VIP cell rhythm is anti-correlated to that of sleep spindle activity
- VIP interneuron activity acutely increases during spindle and slow-oscillation events
- The infraslow VIP rhythm is stronger, overriding acute spindle-associated calcium upregulation



## Article

# VIP interneuron activity during sleep conveys the cortical infraslow oscillation

Kilian Rolle,<sup>1,6</sup> Louisa Weber,<sup>1,6</sup> Jan Born,<sup>1,2,3,4</sup> and Niels Niethard<sup>1,2,5,7,\*</sup>

<sup>1</sup>Institute of Medical Psychology and Behavioral Neurobiology, University of Tübingen, Tübingen, 72076 BW, Germany

<sup>2</sup>German Center for Diabetes Research (DZD) - Institute for Diabetes Research and Metabolic Diseases of the Helmholtz Center Munich at the University Tübingen (IDM), Tübingen, 72076 BW, Germany

<sup>3</sup>German Center for Mental Health (DZPG), Tübingen, 72076 BW, Germany

<sup>4</sup>Center for Integrative Neuroscience, University of Tübingen, Tübingen, 72076 BW, Germany

<sup>5</sup>Department of Cognitive Sciences, University of California, Irvine, Irvine, CA 92617, USA

<sup>6</sup>These authors contributed equally

<sup>7</sup>Lead contact

\*Correspondence: [niels.niethard@uni-tuebingen.de](mailto:niels.niethard@uni-tuebingen.de)

<https://doi.org/10.1016/j.celrep.2025.116669>

## SUMMARY

Sleep is characterized by a specific regulation of cortical circuits that enables plasticity underlying memory consolidation. Vasoactive intestinal polypeptide (VIP)-positive interneurons exert high-level control over cortical activity by inhibiting parvalbumin (PV) and somatostatin (SST)-positive interneurons, thereby disinhibiting pyramidal cells. We used *in vivo* two-photon  $\text{Ca}^{2+}$  imaging to quantify the activity of layer 2/3 VIP interneurons in naturally sleeping male mice during wake, slow-wave sleep (SWS), and rapid-eye-movement (REM) sleep, as well as during spindles and slow oscillations (SOs). VIP activity was lowest during SWS and acutely upregulated during spindles and SOs, presumably facilitating memory processing in cortical circuits. Notably, across all states, VIP activity showed a profound  $\sim 0.02$ -Hz infraslow rhythm, which, during SWS epochs, was inversely phase-coupled to the infraslow rhythm of spindle activity. In contrast, such coupling was absent in SST and PV interneurons, suggesting that VIP cells uniquely regulate infraslow spindle-related dynamics within cortical circuits.

## INTRODUCTION

Sleep is characterized by a distinct regulation of cortical activity that is thought to support plasticity underlying synaptic homeostasis and memory consolidation.<sup>1–3</sup> This regulation is specific to the stages of slow-wave sleep (SWS) and rapid-eye-movement (REM) sleep and is controlled by oscillatory electroencephalography (EEG) events hallmarking these stages: i.e., the slow oscillations (SOs; 0.1–2 Hz) and sleep spindles (11–16 Hz) that occur during SWS, organized within an infraslow rhythm ( $\sim 0.02$  Hz) separating SWS into phases with higher and lower spindle activity. In contrast, REM sleep is dominated by theta oscillations (6–9 Hz).<sup>3–5</sup>

SOs are thalamo-cortical oscillations with alternating down- and upstates, where the downstate involves widespread neuronal hyperpolarization and reduced activity, and the upstate involves depolarization and increased activity.<sup>4,6,7</sup> Sleep spindles promote long-term potentiation<sup>8</sup> and often nest within the SO upstate (i.e., a configuration that is particularly effective in supporting memory consolidation during sleep).<sup>9–11</sup> The cortical circuit mechanisms underlying these oscillatory events are not clear. The initiation of the SO downstate involves increased activity of somatostatin (SST)-positive interneurons, mainly inhibiting the distal dendrites of cortical (layer 2/3) pyramidal cells.<sup>12</sup>

Spindles, on the other hand, are associated with an enhanced soma-targeted inhibition by parvalbumin (PV)-positive interneurons, alongside reduced distal dendritic inhibition resulting from decreased SST cell activity.<sup>12–14</sup> Together, these dynamics appear to create a temporally defined window that facilitates dendritic plasticity in local cortical circuits.<sup>12,15</sup>

Vasoactive intestinal polypeptide (VIP)-positive interneurons represent a third, smaller fraction of interneurons that are well positioned to locally modulate sleep oscillations and associated cortical plasticity, as these cells can inhibit both PV and SST interneurons resulting in a disinhibition of the pyramidal cell.<sup>16</sup> VIP interneurons receive long-range excitatory intra- and extracortical inputs,<sup>17</sup> and their inhibitory effects on PV and SST cells are modulated in a firing-rate-dependent manner<sup>16,18</sup> (i.e., conditions that probably produce distinct temporal dynamics in the interaction between these interneurons). During sleep, activity of layer 2/3 VIP interneurons was found to be synchronized to the oscillations of spindle events, although their average activity during these events remained unchanged.<sup>19</sup> VIP cell activity during REM sleep was generally enhanced.<sup>20</sup>

Here, we aimed at characterizing cortical layer 2/3 VIP interneuron activity during SWS and REM sleep as well as during oscillations known to be involved in regulating memory and plasticity during sleep, i.e., SOs, spindles, and their modulation by



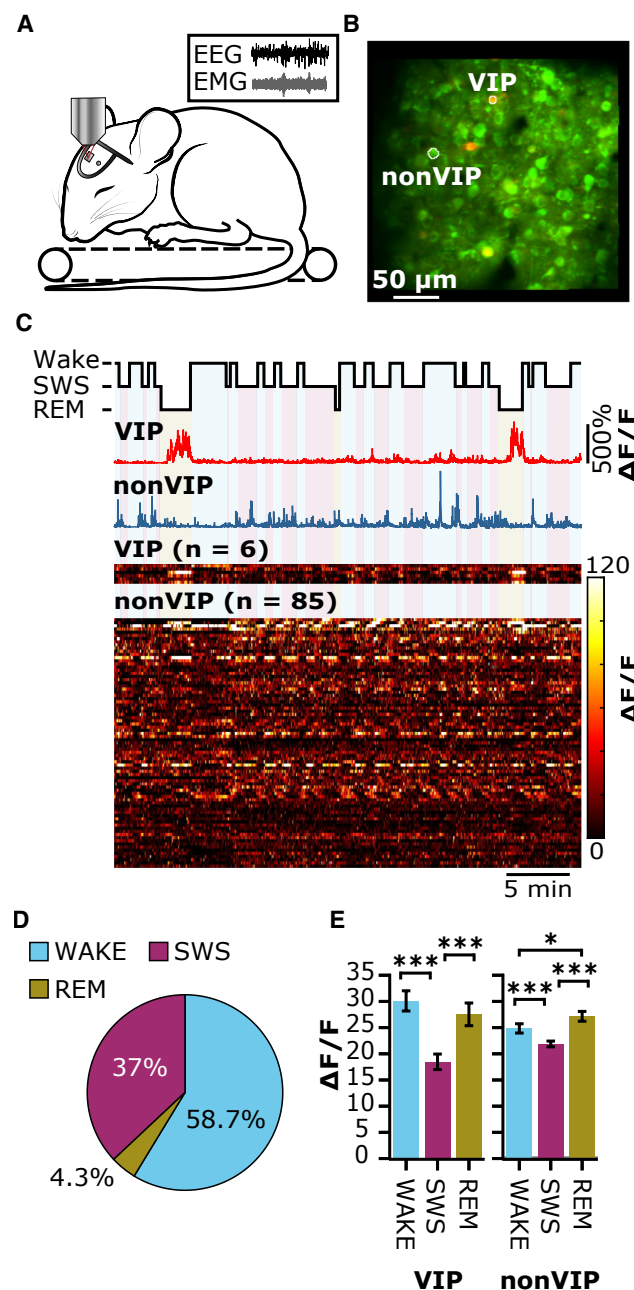


**Figure 1. Sleep-stage-specific  $\text{Ca}^{2+}$  activity in VIP and non-VIP cell populations**

(A) Illustration of the experimental setup.

(B) Example field of view from a composite two-photon recording. The green channel is a maximum-intensity projection of GCaMP8m, and the red channel is the first recording frame of the tdTomato VIP cell labeling. Scale bars indicate 50  $\mu\text{m}$ . Two regions of interest are highlighted, corresponding to the  $\text{Ca}^{2+}$  traces in (C).

(C) Example baseline normalized fluorescence traces ( $\Delta\text{F}/\text{F}$ ) of one VIP neuron (red) and one non-VIP neuron (blue) and a heatmap illustrating the respective population calcium activity (below) corresponding to the respective sleep stages: wake (cyan), slow-wave sleep (SWS, purple), and rapid-eye-movement (REM, gold) sleep (bottom) during 50 min of the recording session.

the  $\sim 0.02$ -Hz infraslow rhythm. Using two-photon  $\text{Ca}^{2+}$  imaging in naturally sleeping mice, we compared  $\text{Ca}^{2+}$  transients of VIP-positive and VIP-negative (non-VIP) cells. Our results reveal a distinct profile for VIP cells, with decreasing activity of VIP cells during SWS episodes but increasing activity within REM sleep epochs. Moreover, VIP interneurons show enhanced activity during spindles and SO down- and upstates, possibly facilitating memory processing in cortical circuits. Importantly, we found VIP interneuron activity to follow a pronounced  $\sim 0.02$ -Hz infraslow rhythm during wake, SWS, and REM sleep. During SWS epochs, this infraslow rhythm was inversely coupled to spindle infraslow activity. To assess the cell-type specificity of this rhythm, we also analyzed infraslow dynamics in the activity of SST and PV interneurons. Compared with VIP interneurons, SST interneurons showed a weaker and temporally shifted coupling to the infraslow rhythm of spindle activity, while PV interneurons exhibited no such coupling.

## RESULTS

### Sleep-stage-specific modulation of VIP and non-VIP activity

We conducted two-photon  $\text{Ca}^{2+}$  imaging of layer 2/3 neurons in the sensorimotor cortex (depth, 150–250  $\mu\text{m}$ ; 1.1 mm caudal and 1–1.3 mm lateral to bregma) during naturally occurring sleep in head-fixed mice. To distinguish between the three major classes of cortical interneurons, we used VIP-, PV-, and SST-Cre mouse lines (see STAR Methods for details). We simultaneously recorded EEG signals contralateral to the imaging site and electromyography (EMG) signals from neck muscles.

First, we examined how sleep stages affect cortical  $\text{Ca}^{2+}$  activity, reflected by the average  $\Delta\text{F}/\text{F}$  for each identified VIP and non-VIP neuron (Figures 1 and S1). In total, our analyses relied on 1,265 wake epochs, 1,411 SWS epochs, and 121 REM sleep epochs (with respective total durations of 2,452.55, 1,545.37, and 179.73 min, recorded during natural sleep under head fixation, nine animals) from 1,341 neurons entailing 124 VIP and 1,217 non-VIP neurons (for the contributions of individual animals, see Table S1). The durations of the recording sessions ( $n = 26$ ) ranged from 37 to 359 min. Activity of VIP cells was correlated between wake and SWS ( $r_{\text{pb}} = 0.56$ ,  $p < 0.001$ ), wake and REM sleep ( $r_{\text{pb}} = 0.44$ ,  $p < 0.001$ ), and SWS and REM sleep ( $r_{\text{pb}} = 0.33$ ,  $p < 0.001$ ). Respective correlations for non-VIP cell activity were, for wake and SWS,  $r_{\text{pb}} = 0.71$  ( $p < 0.001$ ); wake and REM sleep,  $r_{\text{pb}} = 0.49$  ( $p < 0.001$ ); and SWS and REM sleep,  $r_{\text{pb}} = 0.57$  ( $p < 0.001$ ). In a supplementary analysis, we correlated mean VIP activity across animals ( $n = 8$  complete cases) between wake and SWS ( $r_{\text{pb}} = 0.76$ ,  $p = 0.027$ ). The relationship is uncorrelated between wake and REM sleep ( $r_{\text{pb}} = 0.11$ ) or SWS and REM sleep ( $r_{\text{pb}} = -0.077$ ; all  $p > 0.803$ ). Respective correlations for

(D) The percentage of time spent in wake, SWS, and REM sleep (across all sessions) with total recording time set to 100% (see Table S1 for the contribution of individual animals).

(E) Mean ( $\pm$ SEM) percentage of  $\Delta\text{F}/\text{F}$  for each sleep stage for VIP cells ( $n = 124$ , left) and non-VIP cells ( $n = 1217$ , right).

See Figure S1 for the  $\Delta\text{F}/\text{F}$  signals across stage transitions. \* $p < 0.050$ , \*\*\* $p < 0.001$ .

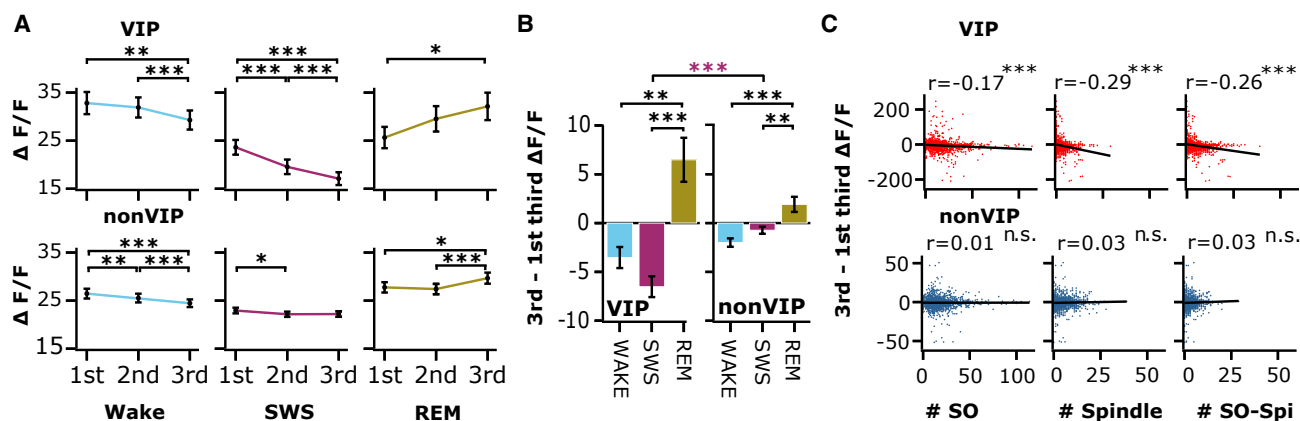


**Figure 2. Within-epoch dynamics of  $\text{Ca}^{2+}$  activity: SWS downregulates and REM sleep upregulates VIP activity**

(A) Mean ( $\pm$ SEM)  $\Delta F/F$  of VIP ( $n = 124$ , top) and non-VIP ( $n = 1217$ , bottom) across thirds of wake (cyan), SWS (purple), and REM (gold) sleep epochs.

(B) Mean ( $\pm$ SEM) differences in  $\Delta F/F$  between 1st and 3rd third of wake, SWS, and REM epochs for VIP (left) and non-VIP cells (right).

(C) Scatterplot illustrating for VIP (upper panels) and non-VIP cells (lower panels) correlations between the within-epoch change in  $\Delta F/F$  (3rd–1st third of epoch) and the number of solitary SOs, spindles, and combined SO-spindle (SO-Spi) events during SWS epochs. Percentage bend correlation coefficients are indicated. See Figure S2 for additional correlations of within episode dynamics. \* $p < 0.05$ , \*\* $p < 0.01$ , \*\*\* $p < 0.001$ .

non-VIP activity were, for wake and SWS,  $r_{pb} = 0.83$  ( $p = 0.011$ ); wake and REM sleep,  $r_{pb} = 0.51$  ( $p = 0.198$ ); and SWS and REM sleep,  $r_{pb} = 0.73$  ( $p = 0.039$ ).

Against this backdrop, there was clear sleep-stage-specific activation of cells that differed between VIP and non-VIP neurons ( $F(2, 2678) = 0.006$ , for the interaction VIP/non-VIP  $\times$  wake/SWS/REM; Figure 1E). VIP cells showed distinctly decreased activity during SWS compared to wake ( $t(123) = -6.58$ ,  $p < 0.001$ ,  $d = -0.60$ ) and REM sleep epochs ( $t(123) = -3.76$ ,  $p < 0.001$ ,  $d = -0.44$ ), whereas activity was comparable between wake and REM sleep ( $t(123) = -1.20$ ,  $p = 0.231$ ,  $F(2, 246) = 16.59$ ,  $p < 0.001$ , for main effect of stage). Non-VIP cells, on the other hand, showed highest  $\text{Ca}^{2+}$  activity during REM sleep (vs. wake:  $t(1216) = 2.30$ ,  $p = 0.043$ ,  $d = 0.07$ ; vs., SWS:  $t(1216) = -6.38$ ,  $p < 0.001$ ,  $d = -0.20$ ), whereas activity was slightly decreased in SWS compared to wake ( $t(1216) = -4.50$ ,  $p < 0.001$ ,  $d = -0.12$ ,  $F(2, 2432) = 19.74$ ,  $p < 0.001$  for stage main effect).

### VIP cell activity decreases within SWS epochs but increases within REM sleep epochs

Next, we investigated how  $\text{Ca}^{2+}$  activity changed *within* individual wake, SWS, and REM sleep epochs by comparing activity during the 1<sup>st</sup>, 2<sup>nd</sup>, and 3<sup>rd</sup> third of each epoch. Again, VIP and non-VIP cells displayed distinguishable activity dynamics during the sleep stages ( $F(2, 2,534) = 3.80$ ,  $p = 0.022$ , for VIP/non-VIP  $\times$  stage; Figure 2A). VIP cells downregulated their activity in the course of wake ( $F(2, 282) = 9.07$ ,  $p < 0.001$ ) and SWS ( $F(2, 282) = 30.95$ ,  $p < 0.001$ ) epochs, whereas they upregulated activity within REM epochs ( $F(2, 234) = 6.26$ ,  $p = 0.005$ ). Non-VIP cells slightly decreased their activity within wake epochs ( $F(2, 2,710) = 15.60$ ,  $p < 0.001$ ) and increased activity within REM sleep epochs ( $F(2, 2,300) = 6.53$ ,  $p = 0.002$ ,  $F(2, 2,534) = 20.81$ ,  $p < 0.001$  for main effect of stage).

Additional analyses on the difference in activity between the 1<sup>st</sup> and 3<sup>rd</sup> third of an epoch confirmed that VIP cells upregulated

activity during REM epochs when compared to both SWS ( $t(117) = -5.80$ ,  $p < 0.001$ ,  $d = 0.74$ ) and wake epochs ( $t(117) = 3.72$ ,  $p = 0.001$ ,  $d = 0.52$ ,  $F(2, 234) = 18.41$ ,  $p < 0.001$ , for main effect of stage; Figure 2B). The downregulation of VIP  $\Delta F/F$  within SWS epochs did not differ from that during wake epochs ( $t(117) = -1.98$ ,  $p = 0.100$ ) but was more pronounced than in non-VIP cells during SWS ( $t(145) = 5.97$ ,  $p < 0.001$ ,  $d = 0.55$ ;  $F(2, 2,534) = 8.84$ ,  $p < 0.001$ , for VIP/non-VIP  $\times$  stage interaction). The REM-associated upregulation of VIP cells did not differ from that in non-VIP cells ( $p = 0.115$ ).

### The link of within-epoch changes in $\text{Ca}^{2+}$ activity to epoch duration, EEG power, and oscillatory events

Correlation analyses revealed that changes in  $\text{Ca}^{2+}$  activity of VIP cells within SWS epochs were marginally but significantly negatively correlated with the duration of these epochs ( $r_{pb} = -0.07$ ,  $n = 1,411$ ,  $p = 0.011$ ); i.e., the longer the epoch duration, the stronger the decrease in  $\text{Ca}^{2+}$  activity from the 1<sup>st</sup> to the 3<sup>rd</sup> third of the epoch (Figure S2A). Non-VIP cells, in contrast, showed a positive correlation ( $r_{pb} = 0.05$ ,  $n = 1,411$ ,  $p < 0.050$ ). Notably, for REM sleep epochs, the relationships of within-stage changes in  $\text{Ca}^{2+}$  activity with epoch duration were much more pronounced and, for non-VIP cells, even in the opposite direction to those for SWS epochs. Here, with longer REM epoch duration, the increase in  $\text{Ca}^{2+}$  activity of VIP cells was less pronounced than in epochs of shorter duration ( $r_{pb} = -0.50$ ,  $n = 121$ ,  $p < 0.001$ ; Figure S2A). This negative correlation was distinctly weaker for non-VIP cells ( $r_{pb} = -0.27$ ,  $n = 121$ ,  $p = 0.003$ ;  $z = 2.05$ ,  $p = 0.041$ , for the comparison between VIP and non-VIP cells).

Correlations with EEG power did not reveal hints that the within-epoch changes in VIP cell activity specifically depended on the EEG frequencies hallmarking SWS and REM sleep, respectively (Figure S2B and S2C). During SWS epochs, mean power in the 0.5- to 4-Hz slow-wave activity (SWA) band was weakly but significantly negatively correlated with VIP  $\text{Ca}^{2+}$



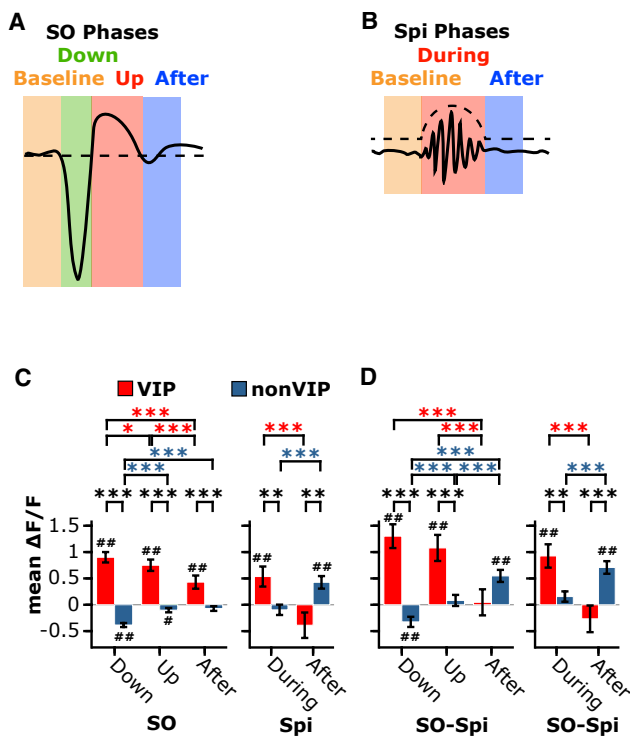


**Figure 3. Acute changes in VIP cell activity during solitary SOs, spindles, and SO-spindle events**

(A and B) (A) Schematic illustration of phases analyzed for (A) slow-oscillation (SO) and (B) spindle events.

(C) Baseline-corrected  $\text{Ca}^{2+}$  activity for VIP (red) and non-VIP (blue) cell populations during the downstate, upstate, and after phases of solitary SOs (left) and the during and after phases of solitary spindles (right).

(D) Left: activity during the downstate, upstate, and after phases of SO-spindle events. The phases are defined with reference to the SO of the SO-spindle events. Right: results from an analysis focusing on the during and after phases of the spindle nesting in the respective SO-spindle events. The phases are defined with reference to the nested spindle. Means ( $\pm$ SEM) are indicated (see Table S2 for the contribution of individual animals).

\* $p < 0.05$ , \*\* $p < 0.01$ , \*\*\* $p < 0.001$ , for *post hoc* pairwise comparisons. Significance against baseline level: # $p < 0.05$ , ## $p < 0.01$ .

changes (from 1<sup>st</sup> to 3<sup>rd</sup> third,  $r_{pb} = -0.08$ ,  $n = 1,411$ ,  $p = 0.002$ ). Similar, partly even stronger negative correlations were obtained for the neighboring 6- to 9-Hz theta (VIP cells:  $r_{pb} = -0.20$ ,  $n = 1,411$ ,  $p < 0.001$ . Non-VIP cells:  $r_{pb} = -0.08$ ,  $n = 1,411$ ,  $p = 0.002$ ) and the 11- to 16-Hz sigma bands (VIP:  $r_{pb} = -0.31$ ,  $n = 1,411$ ,  $p < 0.001$ . Non-VIP:  $r_{pb} = -0.06$ ,  $n = 1,411$ ,  $p = 0.033$ ). Opposing the correlations in SWS,  $\text{Ca}^{2+}$  dynamics within REM sleep epochs were consistently positively correlated with mean power in the 6- to 9-Hz theta band as well as in the 0.5- to 4-Hz SWA and 11- to 16-Hz sigma bands (for both VIP and non-VIP cells,  $r_{pb} \geq 0.26$ ,  $p \leq 0.004$ ).

SOs and spindles, particularly spindles that occur during the SO upstate (SO-spindle events), are crucial for memory consolidation during SWS.<sup>3,9</sup> Counts of all three event types, solitary SOs (i.e., SOs without nested spindles), solitary spindles (spindles occurring outside an SO upstate), and coupled SO-spindle events (SOs that nest a spindle in the upstate), were negatively

correlated with changes in VIP cell activity within SWS epochs, with the strongest correlations for counts of solitary spindles ( $r_{pb} = -0.29$ ;  $n = 1,411$ ,  $p < 0.001$ ; Figure 2C). Changes in non-VIP  $\text{Ca}^{2+}$  activity did not show any significant correlation with these events (all  $p \geq 0.268$ ).

### VIP cell activity is acutely upregulated during SOs and spindles

We examined the instantaneous  $\text{Ca}^{2+}$  activity of VIP and non-VIP cells during the occurrence of SO and spindle events. Analyses were performed on a total of 15,892 solitary SO events, 2,512 solitary spindle events, and 2,288 combined SO-spindle events (Table S2). Activity was assessed with reference to average activity during a  $-1$ -s to  $-0.5$ -s baseline interval preceding the event for three phases of the SO (i.e., the downstate, upstate, and a 750-ms after phase; Figure 3A), as well as during and after spindle events (Figure 3B).

Solitary SO events were characterized by specific acute temporal dynamics of  $\text{Ca}^{2+}$  activity of VIP cells, in comparison with that of non-VIP cells ( $F(3, 47,601) = 48.31$ ,  $p < 0.001$ , for VIP/non-VIP  $\times$  phase). Importantly, on top of a generally reduced activity during SO events, VIP cells exhibited maximal activity during the SO downstate, which only slightly decreased during the subsequent upstate ( $t(15,867) = 1.99$ ,  $p = 0.047$ ,  $d = 0.01$ ), and further decreased during the after phase ( $t(15,867) = -4.30$ ,  $p < 0.001$ ,  $d = 0.03$ ). This contrasts with the dynamics in non-VIP cells, which showed minimal activity during the SO downstate (see Figure 3C for pairwise statistical comparisons). During solitary spindles,  $\text{Ca}^{2+}$  activity was higher in VIP than non-VIP cells ( $t(5,022) = -2.95$ ,  $p = 0.005$ ,  $d = -0.08$ ), and this pattern inverted in the after phase of the spindle ( $t(5,022) = 3.02$ ,  $p = 0.005$ ,  $d = 0.09$ ; Figure 3C).

In SOs co-occurring with a spindle (i.e., SO-spindle events), the dynamics obtained for solitary SO events were, on average, enhanced, although this enhancement did not reach significance. Thus, VIP cell activity in the downstate phase of these SO-spindle events was profoundly increased above baseline levels (against baseline:  $t(2,283) = 5.80$ ,  $p < 0.001$ ,  $d = 0.17$ ; vs. non-VIP:  $t(2,283) = -6.60$ ,  $p < 0.001$ ,  $d = -0.20$ ) but still not significantly different from activity during the downstate phase of solitary SO events ( $p = 0.308$ ; Figure 3D). Focusing the analysis of SO-spindle events on the interval of the nested spindle revealed that  $\text{Ca}^{2+}$  activity of VIP cells was also profoundly enhanced during the spindle ( $t(2,287) = 4.18$ ,  $p < 0.001$ ,  $d = 0.12$  against baseline,  $t(4,574) = -3.18$ ,  $p = 0.002$ ,  $d = -0.09$  vs. non-VIP,  $t(4,618) = 1.34$ ,  $p = 0.364$  vs. VIP activity during solitary spindles; Figure 3D).

### VIP interneuron activity during SWS exhibits a $\sim 0.02$ infraslow oscillation with an inverse phase to that of spindle activity

For each SWS epoch, we calculated autocorrelation functions (ACFs) of mean activity across all VIP and non-VIP cells, respectively (bin size, 235 ms). ACFs for mean VIP cell activity displayed a prominent negative peak at 24 s ( $zr = -0.25$ ) followed by a smaller positive peak at 59 s ( $zr = 0.06$ ), reflecting an infraslow oscillation with a period length of  $\sim 50$  s (Figures 4A and 4B). ACFs for non-VIP cell activity revealed a similar but distinctly

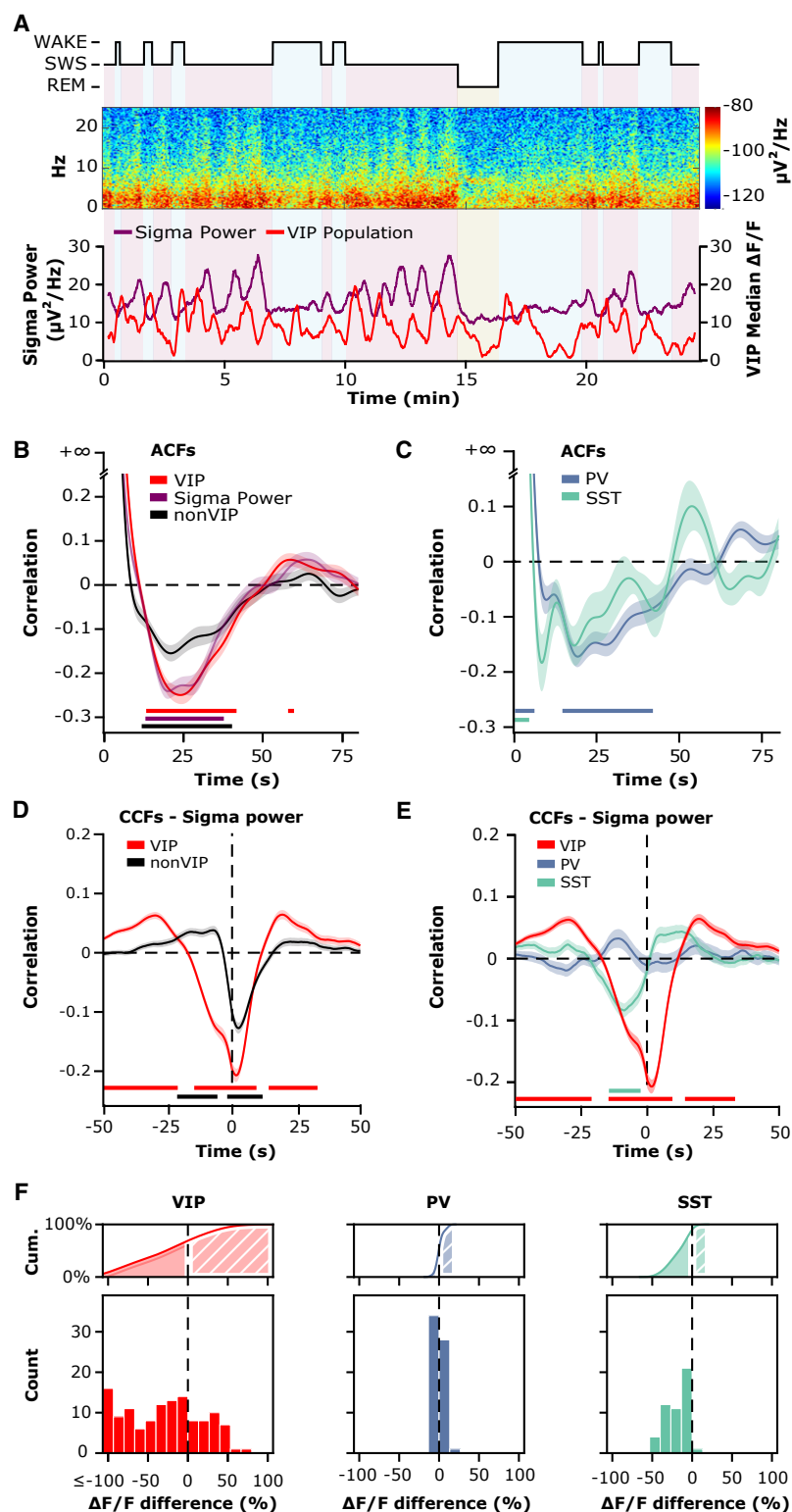


**Figure 4. VIP cell activity during SWS epochs shows an  $\sim 0.02$ -Hz infraslow oscillation**

(A) Example recording from a 25-min session showing (from top to bottom) sleep-stage profile (wake, cyan; SWS, magenta; REM sleep, gold), the corresponding EEG spectral power, and the traces of average VIP population  $Ca^{2+}$  activity (red) and 11- to 16-Hz EEG sigma power (purple, both signals smoothed by a 20-s moving average). Note pronounced  $\sim 0.02$ -Hz infraslow rhythm of VIP cell activity during SWS epochs, which is also visible in REM sleep and wake epochs, although with distinctly lower amplitude. During SWS, the infraslow oscillations in VIP cell activity exhibit an inverse phase relationship to those in EEG sigma activity, with decreases in VIP cell activity occurring with increases in sigma activity.

(B) Mean ( $\pm$ SEM) autocorrelation function (ACF) for  $Ca^{2+}$  activity of VIP (red) and non-VIP (black) cell populations and EEG sigma (11–16 Hz) power (purple) during SWS epochs ( $n = 97$  epochs with durations  $\geq 120$  s).

(C) ACFs of PV cell (blue)  $Ca^{2+}$  activity, calculated during ( $n = 56$ ) SWS epochs, and SST cell (green)  $Ca^{2+}$  activity calculated during ( $n = 16$ ) SWS epochs, each of at least 120-s duration.

(D) Mean ( $\pm$ SEM) cross-correlation functions (CCFs) between 11- and 16-Hz EEG sigma power and  $Ca^{2+}$  activity of VIP (red) and non-VIP cells (blue) during  $n = 789$  SWS epochs (with durations  $\geq 50$  s). Note that the negative peak of the CCF for VIP cell activity around 0 s indicates an inverse phase relationship between infraslow oscillations in sigma power and VIP cell activity. See Figure S3 for CCFs during other sleep stages.

(E) Mean ( $\pm$ SEM) CCFs between 11- and 16-Hz EEG sigma power and  $Ca^{2+}$  activity of VIP (red), PV (blue), and SST cells (green) during SWS epochs (with durations  $\geq 50$  s). Note the pronounced negative peak (around 1.65 s) of CCF between VIP cell activity and sigma activity, reflecting an inverse relationship between the infraslow rhythms of both parameters. No similar patterns are observed for the CCFs for PV and SST cell activity. Colored horizontal bars at the bottom indicate significant correlation coefficients ( $p < 0.05$  after Bonferroni-Holm correction).

(F) Cumulative density plots (top row) showing cell-wise modulation of  $\Delta F/F$  signals, computed as the difference between mean activity during the positive vs. negative half-wave of the infraslow sigma oscillation. Corresponding histograms (bottom row) illustrate the distribution of this modulation for VIP (left), PV (middle), and SST (right) cells. VIP cells with values  $\leq 100$  were binned together. The dashed vertical line marks zero, separating cells preferentially active during the negative or positive half-wave. Most SST (98.0%) and VIP (71.8%) interneurons show negative values, indicating higher activity during the negative half-wave, whereas PV (53.2%) interneurons are symmetrically distributed around zero, showing no consistent modulation by the infraslow sigma oscillation.

flatter oscillation with peak negative coefficients at 21 s and peak positive coefficients at 65 s ( $zr = -0.15$ ). Comparing the peak negative coefficients at the respective time lags confirmed that

the ACFs of VIP cell activity ( $t(96) = -3.31$ ,  $p = 0.001$ ,  $d = -0.34$ ), and also the subsequent positive peak coefficient tended to be still higher in

this negative peak was distinctly higher for the VIP than non-VIP cell ACFs ( $t(96) = -3.31$ ,  $p = 0.001$ ,  $d = -0.34$ ), and also the subsequent positive peak coefficient tended to be still higher in

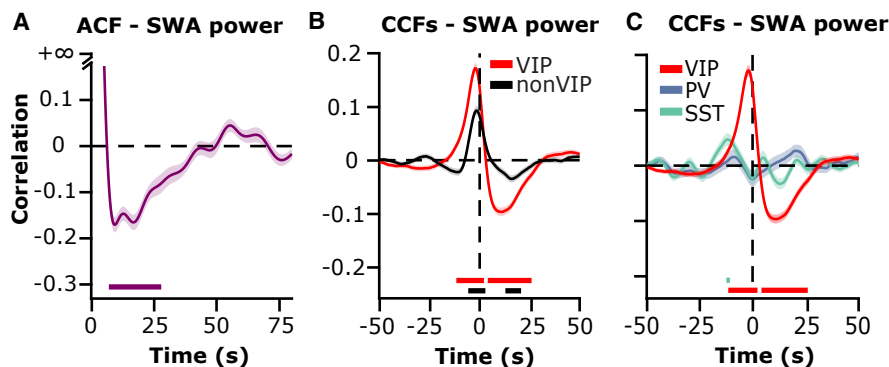


**Figure 5. VIP cell activity is correlated with infraslow modulations of SWA**

(A and B) (A) Mean ( $\pm$ SEM) ACF for EEG power in the 0.5- to 4-Hz SWA band (purple) during SWS epochs ( $n = 97$ ) and (B) corresponding CCFs between SWA power and activity of VIP cells (red) and non-VIP cells (black,  $n = 789$  epochs of  $\geq 50$ -s duration). Note the positive peak of the CCF for VIP cell activity shortly before 0 min, pointing to an in-phase relationship between rhythms of VIP cell activity and SWA.

(C) Mean ( $\pm$ SEM) CCFs between 0.5- and 4-Hz EEG SWA power and Ca<sup>2+</sup> activity of VIP (red), PV (blue), and SST cells (green) during SWS epochs (with durations  $\geq 50$  s). Colored horizontal bars at the bottom indicate significant correlation coefficients ( $p < 0.05$  after Bonferroni-Holm correction).

tied to a  $\sim 50$ -s oscillation. PV cell activity showed a significant negative peak around 19 s during SWS ( $zr = -0.17$ ), while SST cells did not exhibit any significant peaks in ACFs during SWS (Figure 4C).

To directly compare the infraslow oscillation of VIP activity with the well-known infraslow oscillation of spindle activity,<sup>5</sup> we additionally calculated ACFs for power in the 11–16 Hz EEG sigma band (for the same SWS epochs). Interestingly, these sigma power ACFs were highly comparable to those of VIP cell activity, with a pronounced negative peak at 20 s ( $zr = -0.24$ ) and a subsequent positive peak at 64 s ( $zr = 0.06$ ; Figure 4B). We then calculated cross-correlation functions (CCFs) between the respective time series of VIP Ca<sup>2+</sup> activity and sigma band power (Figure 4D), which revealed a clear negative peak at +1.65 s lag ( $zr = -0.21$ ), indicating an inverse phase relationship between the infraslow oscillations in both time series; i.e., maximum activity of VIP cells is associated with minimum sigma power and vice versa, and minimum sigma power is associated with maximum VIP cell activity (see Figure 4A for an example). For non-VIP cells, corresponding CCFs also showed a negative peak correlation at +2.58 s, which, however, was of distinctly lower magnitude ( $zr = -0.13$ ,  $t(788) = -6.17$ ,  $p < 0.001$ ,  $d = -0.28$ , for the difference to the minimum in the CCFs for VIP cells). VIP cell activity also displayed the most robust cross-correlation pattern with sigma band power during SWS when compared with the respective CCFs for PV and SST interneurons (Figure 4E). For PV cells, the apparent positive CCF peak at  $-11$  s did not survive correction for multiple comparisons ( $zr = 0.03$ ,  $p_{unc} = 0.034$ ), and SST cells showed a less pronounced negative peak in their CCFs at  $-8.79$  s ( $zr = -0.08$ ,  $p < 0.001$ ) compared to VIP cells.

In addition, we investigated the participation of individual cells in this modulation during SWS. We found that the majority of VIP interneurons (71.8%) exhibited higher mean Ca<sup>2+</sup> activity levels during the troughs of the infraslow sigma oscillation than during the peaks ( $W(124) = 1,592$ ,  $p < .001$ ; Figure 4F). A similar pattern was even more pronounced for SST interneurons (98.0%,

$W(49) = 2$ ,  $p < 0.001$ ). In contrast, PV interneurons showed no clear activity preference (52.2%  $W(63) = 912$ ,  $p = 0.513$ ).

We also examined the relationship of the  $\sim 0.02$ -Hz infraslow oscillation of VIP cell activity during SWS epochs to power in the 0.5- to 4-Hz SWA band (covering the SO events). ACFs for SWA power revealed a broader minimum with a first negative peak at 9 s ( $zr = -0.17$ ,  $p < 0.001$ ), i.e., distinctly earlier than ACFs for sigma power, with a subsequent positive peak around 56 s, which did not reach significance ( $zr = 0.04$ ,  $p = 0.412$ ; Figure 5A). These results agree with previous findings,<sup>5</sup> indicating that the  $\sim 0.02$ -Hz infraslow rhythm characterizing sigma power is less well expressed in SWA ( $t(96) = -2.96$ ,  $p = 0.004$ ,  $d = -0.30$ , for the difference between the minimum correlations in the ACFs for sigma and SWA power). Moreover, opposite to CCFs for sigma power, CCFs between the time series of SWA and VIP cell activity showed maximum positive coefficients shortly before the zero-time lag ( $-2.12$  s;  $zr = 0.17$ ,  $p < 0.001$ ; Figure 5B); i.e., here, maximum VIP cell activity was accompanied by maximum rather than minimum SWA, and vice versa. The activity of non-VIP cells showed the same relationship to SWA power but less pronounced than in VIP cells ( $-1.41$  s,  $zr = 0.09$ ,  $t(788) = 6.72$ ,  $p < 0.001$ ,  $d = -0.30$ , compared with the respective correlation in CCFs for VIP cells; Figure 5B). CCFs between SWA and PV activity revealed no significant peak. For SST cells, CCFs only showed a single positive peak at  $-12.17$  s ( $zr = 0.05$ ;  $p < 0.001$ ; Figure 5C).

### The infraslow rhythm in VIP cells, but not in EEG sigma activity, is independent of SWS

The inverse coupling of the infraslow oscillation of VIP cell activity with EEG sigma power was specific to SWS epochs. Importantly, ACFs for VIP cell activity showed a pronounced negative peak (around 23 s) also during REM sleep epochs and wake epochs, which was closely comparable to that observed during SWS epochs ( $p > 0.121$  for the difference in the minima between the three stages; Figure 6A), overall indicating that the  $\sim 0.02$ -Hz infraslow rhythm of VIP cell activity persists during REM sleep as

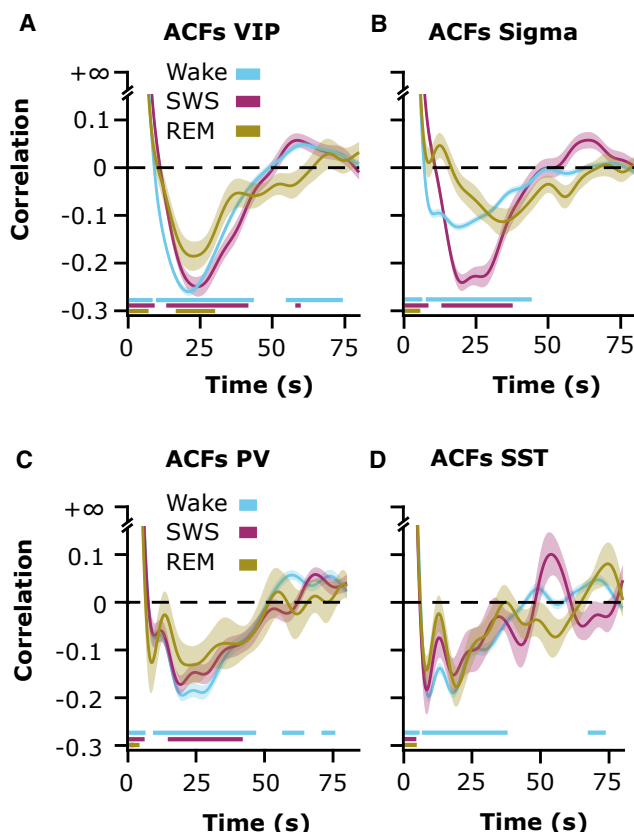


**Figure 6. The  $\sim 0.02$ -Hz infraslow oscillation in VIP cell activity persists during sleep and wake states**

(A and B) Mean ( $\pm$ SEM) ACFs for (A) VIP cell  $Ca^{2+}$  activity and (B) EEG 11- to 16-Hz sigma power, calculated during wake (cyan,  $n = 394$ ), SWS (purple,  $n = 97$ ), and REM sleep (gold,  $n = 30$ ) epochs of at least 120-s duration. Note the highly comparable ACFs for VIP cell activity in all three brain states. ACFs for EEG sigma band, on the other hand, indicate a significant negative peak (around 21 s) only during SWS epochs, reflecting that the presence of the infraslow rhythm in sigma-band activity is restricted to SWS. (C) Mean ( $\pm$ SEM) PV cell  $Ca^{2+}$ -activity ACFs, calculated during wake (cyan,  $n = 106$ ), SWS (purple,  $n = 56$ ), and REM sleep (gold,  $n = 14$ ) epochs, and (D) SST cell  $Ca^{2+}$ -activity ACFs calculated during wake (cyan,  $n = 143$ ), SWS (purple,  $n = 16$ ), and REM sleep (gold,  $n = 15$ ) epochs each of at least 120-s duration. Colored horizontal bars at the bottom indicate significant correlation coefficients ( $p < 0.05$  after Bonferroni-Holm correction).

well as wake epochs. Direct comparisons of the infraslow oscillation amplitudes between states revealed lower amplitudes during REM sleep compared to SWS ( $t(235) = -3.38$ ,  $p = 0.003$ ,  $d = -0.19$ ) or wake ( $t(181) = -5.54$ ,  $p < 0.001$ ,  $d = -0.33$ ) and moderately higher during wake than SWS ( $t(1,577) = -2.07$ ,  $p < 0.038$ ,  $d = -0.10$ ;  $F(2) = 4.77$ ,  $p = 0.009$  for the main effect of stage). In contrast, ACFs for sigma power during REM sleep epochs as well as wake epochs were quite different from those during SWS epochs and did not indicate any distinct minima or maxima (Figure 6B), in line with the view that the infraslow rhythm in EEG sigma activity is specific to SWS epochs (e.g., Osorio-Forero et al.<sup>21</sup>). Accordingly, CCFs did not provide evidence of a specifically timed relationship of sigma power to VIP cell activity in REM sleep or wake epochs (Figure S3). As to the other inter-

neuron types, PV cell ACFs showed a comparable  $\sim 0.02$ -Hz rhythm during wake and SWS but not during REM epochs (Figure 6C;  $F(2) = 3.89$ ,  $p = 0.021$  for the main effect of stage). For SST cell activity, ACFs revealed significant infraslow modulations only during wake but not during SWS or REM sleep (Figure 6D).

### The infraslow oscillation in VIP cell activity exceeds the acute upregulation of VIP cell activity during spindle events

In order to estimate the relative contributions of the infraslow oscillation and of the acute upregulation of VIP cell activity during spindle and SO events, we calculated event-correlation histograms averaging VIP  $Ca^{2+}$  activity, i.e., the  $\Delta F/F$  signal, unreferenced to any baseline in a  $\pm 50$ -s interval around solitary spindle and SO events, respectively (Figure 7). These histograms indicate strong, slow dynamics in VIP but not in non-VIP cell activity around the events of interest that completely masked the acute upregulation of VIP cell activity during SO and spindle events (as observed when the  $\Delta F/F$  signal is adjusted to a pre-event baseline; Figure 3). Notably, the average  $Ca^{2+}$  activity around spindle events exhibits the form of a distinct infraslow oscillation with the spindle events closely timed to the minimum in VIP cell  $Ca^{2+}$  activity (Figure 7A), underlining the strong inverse relationship we observed between infraslow rhythms of VIP cell activity and sigma power (Figures 4D and 4E). Consequently,  $Ca^{2+}$  activity of VIP interneurons within a 20-s interval following a spindle event was distinctly increased (with reference to activity during the event;  $t(175) = -4.84$ ,  $p < 0.001$ ,  $d = 0.18$ ). On the other hand, VIP cell activity was rather decreased in the corresponding 20-s interval following SO events ( $t(1421) = 4.32$ ,  $p < 0.001$ ,  $d = 0.11$ ; Figure 7B), which is consistent with our finding that infraslow oscillations in SWA activity appeared to be coupled in phase with the infraslow rhythm of VIP cell activity (Figures 5B and 5C). Comparing changes in  $Ca^{2+}$  activity at an even slower timescale (i.e., between the first and last 10-s interval of the  $\pm 50$ -s interval around spindle and SO events) revealed a general decrease in VIP cell activity that was independent of whether averages were time locked to solitary spindle or SO events ( $F(1, 1,596) = 0.980$ , for main effect of event type; Figure 7C) consistent with our finding that, within SWS epochs, VIP cell activity is generally decreasing (Figure 2A).

## DISCUSSION

We used *in vivo* two-photon  $Ca^{2+}$  imaging to characterize the activity of cortical VIP interneurons during natural sleep, differentiating activity during the different stages of sleep and wakefulness, as well as during oscillatory signatures of SWS, i.e., SOs, spindles, and the  $\sim 0.02$ -Hz infraslow rhythm, which are known to contribute to memory processing and underlying synaptic plasticity during sleep. VIP interneurons inhibit both SST and PV interneurons<sup>22</sup> and, thereby, are thought to primarily exert a disinhibitory effect on cortical pyramidal cells.<sup>23</sup>

We found that VIP neurons exhibit lowest activity during SWS and increased activity during REM sleep, consistent with previous studies.<sup>19,20</sup> Within SWS, VIP neurons downregulate their activity, whereas, in REM sleep, VIP interneurons upregulate



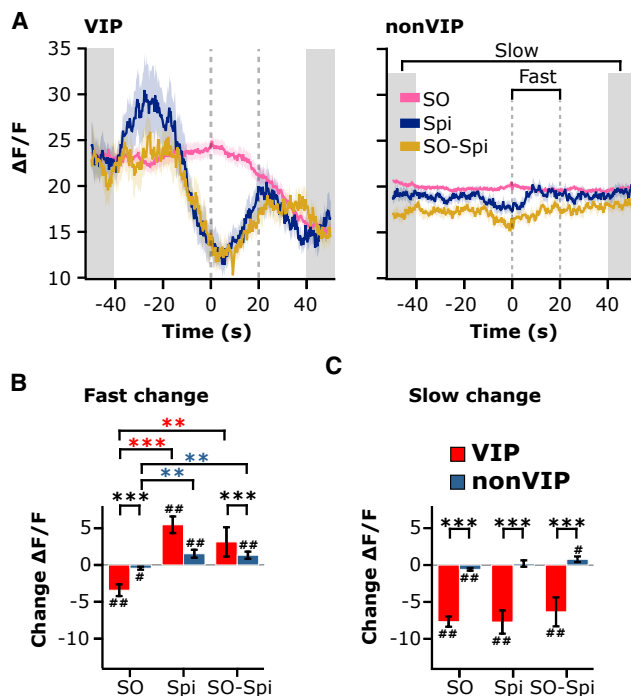


**Figure 7. Infraslow changes in VIP activity dominate around spindle events**

(A) Average  $\Delta F/F$  ( $\pm$ SEM) fluorescence traces of VIP (left) and non-VIP cell activity (right) in a  $\pm 50$ -s interval around solitary spindles ( $n = 176$ , blue), SO events ( $n = 1,422$ , pink), and coupled SO-Spi events ( $n = 157$ , gold). Averaging is time-locked (0 s) to the onset of spindle events and the downstate peak of SO events, respectively. Intervals used for calculating fast and slow changes in (B) and (C) are indicated by dashed lines and gray-shaded areas, respectively. (B) Mean ( $\pm$ SEM) activity of VIP (red) and non-VIP (blue) cell activity in the 20-s interval following solitary SO and spindle events and combined SO-spindle events. Difference values are shown with reference to activity during a 1.2-s interval starting with the SO and spindle event onsets, respectively. (C) Mean ( $\pm$ SEM) VIP (red) and non-VIP (blue) cell activity in the first (–50 to –40 s) and last (+40 to +50 s) 10-s interval of the  $\pm 50$ -s interval around solitary SO and spindles, and SO-spindle events.  $**p < 0.01$ ,  $***p < 0.001$ , for *post hoc* pairwise comparisons. Hashes indicate significance against zero.  $\#p < 0.05$ ,  $##p < 0.01$ .

their activity. The downregulation of VIP cell activity within SWS epochs was stronger in longer epochs and in epochs with high spindle density. Oscillatory analyses revealed a timescale-dependent regulation of VIP activity: acutely, spindles and SO down- and upstates were associated with transient increases in VIP activity, whereas, on a slower timescale, VIP activity in all vigilance states followed a prominent  $\sim 0.02$ -Hz infraslow rhythm. During SWS, this infraslow rhythm is closely coupled to the well-known infraslow rhythm in EEG sigma power, such that, here, phases of maximum VIP activity were associated with minimum spindle activity.

Acutely, VIP cells upregulated activity not only during spindle events but also during SO events, regardless of whether these events occurred in isolation or combination (i.e., as SO-spindle events). Given that these events are well known to support memory consolidation,<sup>3,10,11,24</sup> this event-associated upregulation of VIP cell activity points to an acute involvement of these cells in

supporting underlying plasticity in cortical circuits.<sup>19</sup> The effect might basically be mediated via the inhibitory actions of VIP cells on SST and PV interneurons.<sup>22</sup> Consistent with such inhibition, in previous studies, SST mediating a dendritic inhibition of pyramidal cells showed reduced activity during spindles as well as during the SO downstate, and also PV cells mediating inhibition of the pyramidal cell soma showed reduced activity during SO downstates.<sup>12</sup> However, PV cells were highly active during spindles independently of whether they occurred in isolation or were nested into an SO upstate. Apparently, the increased activity of VIP cells we observed during spindles does not directly translate into a strong and parallel suppression of both SST and PV cells. Instead, the acute regulation of these interneurons may involve additional modulating factors, possibly involving direct thalamo-cortical inputs on VIP and PV cells.<sup>25</sup> Our results suggest that, by acutely inhibiting SST and PV cells during spindles and SOs, VIP cells may bias the function of these interneurons toward reducing the overall inhibition converging onto pyramidal cells and thereby eventually facilitate memory processing and underlying dendritic synaptic plasticity in these circuits.<sup>12,26,27</sup>

We identified a remarkably robust  $\sim 0.02$ -Hz infraslow rhythm in the activity of VIP interneurons as a previously unknown rhythm that is persistently present during wake and SWS and during REM sleep with reduced amplitude. This rhythm was by far more pronounced in the VIP than non-VIP cell population and, during SWS epochs, was closely but inversely coupled with the infraslow rhythm of spindle activity. Comparisons with PV and SST interneurons confirmed that this relationship is specific to VIP cells: the activity of PV cells did not show any significant cross-correlations with sigma band activity, and, for SST cell activity, the respective correlation coefficients were distinctly lower, reaching significance only for a negative peak. This peak, moreover, occurred at a lag of  $-8.79$  s, suggesting that fluctuations in SST cell activity *follow* fluctuations in sigma power, whereas VIP activity preceded them. Infraslow fluctuations at similar timescales that persist across sleep and wake states have been observed using various electrophysiological measures like the cortical steady-state potential and band-limited power modulation of local field potential recordings.<sup>28–30</sup> They have been commonly interpreted as more or less widespread changes in cortical excitability that could be conveyed via cortico-thalamic networks.<sup>31</sup> However, their origin remains unclear. The present findings identify VIP interneurons as potential mediators of such infraslow oscillation in excitability at the cortical level.

During SWS epochs, the coupling of the infraslow rhythm of VIP cell activity appeared to be specific to spindle activity. Thus, coupling to EEG SWA was less pronounced and, additionally, with an opposite phase relationship (i.e., a pattern overall mirroring previous findings on the relationship between infraslow rhythms in SWA and spindle activity).<sup>5,21</sup> Although we observed close temporal coupling of the infraslow rhythm in VIP cell activity with that of spindle activity, we can only speculate about a causal contribution of VIP cells to mediating this sigma rhythm. The infraslow rhythm in sigma activity likely reflects underlying neuromodulatory dynamics operating on a similar timescale. Three neurotransmitters have been implicated in such rhythms during SWS: noradrenaline,<sup>21</sup> acetylcholine,<sup>32</sup> and serotonin.<sup>33</sup>

In particular, noradrenaline<sup>21</sup> and acetylcholine activity<sup>32</sup> were found to correlate negatively with infraslow modulations in sigma band power. All three neuromodulators also influence VIP interneuron activity, either directly, through receptor activation in the case of serotonin<sup>34</sup> and acetylcholine,<sup>35</sup> or indirectly via modulating activity of noradrenergic afferents.<sup>36</sup> Interestingly, although cortical VIP cells receive direct noradrenergic input,<sup>36</sup> the proportion of VIP cells activated following locus coeruleus stimulation is lower than that of PV and SST interneurons.<sup>37</sup> However, in our data, PV and SST cells showed no or only weak cross-correlations with sigma power, which challenges the view that noradrenaline alone mediates the infraslow rhythms in VIP cells and sigma activity but suggests contributions of additional mechanisms. Indeed, VIP cell responses may not only reflect the acute actions of neuromodulators but also integrate the tonic level of activity in the different sleep stages. During SWS, noradrenergic as well as serotonergic activity are at an intermediate level, whereas they are minimal during REM sleep.<sup>38–40</sup> These variations in neuromodulatory tone could well modulate more acute VIP cell responses and, consequently, the extent to which cortical pyramidal cells experience disinhibition.<sup>41</sup>

Regardless of its origin, the infraslow rhythm in VIP cell activity operates in the opposite direction to the acute modulation observed around spindle events, indicating that the infraslow regulation and the acute spindle-associated regulation of VIP cell activity are mediated by distinct pathways. Notably, changes in VIP activity across the infraslow cycle were more than 25-fold larger than those accompanying individual spindles. Consequently, the transient upregulation of VIP cells during a spindle is overridden by the strong infraslow decrease in activity at that phase. The small magnitude of spindle-related VIP activation suggests that, rather than reflecting a diffuse modulatory influence from brainstem neuromodulatory centers, it likely represents a more localized response, potentially arising from intracortical inputs that are restricted to smaller subpopulations of these cells.<sup>16</sup>

### Limitations of the study

Our analyses compared VIP cell activity with that of non-VIP cells, a heterogeneous group that may include subpopulations sharing VIP-like dynamics. Nonetheless, the specificity of the inverse relationship between VIP infraslow activity and spindle activity was supported by additional analyses of PV and SST cells. Another limitation is that our recordings were restricted to cortical layer 2/3, preventing assessment of similar infraslow VIP dynamics in other layers or regions. Moreover, we did not manipulate VIP activity directly, limiting causal inference about their role in spindle regulation.

Despite these constraints, our findings reveal that VIP interneurons display distinct sleep-related activity patterns, dissociable from PV and SST cells both during spindle and SO events—i.e., events critical to memory formation during sleep,<sup>11,12,19,42</sup> as well as with respect to the infraslow regulation of spindle activity. Indeed, the particular dynamic of VIP cell activity around spindles, dominated by an infraslow decrease around these events, may be of particular relevance given recent findings suggesting that the consolidation of new memories dur-

ing SWS relies on neuronal reactivations preferentially occurring during infraslow phases of lowered noradrenergic activity,<sup>43</sup> when spindle activity is presumably high, but activity in the VIP cell population is globally downregulated.

### RESOURCE AVAILABILITY

#### Lead contact

Further information and requests for resources should be directed to the lead contact, Niels Niethard ([niels.niethard@uni-tuebingen.de](mailto:niels.niethard@uni-tuebingen.de)).

#### Materials availability

This study did not generate new reagents.

#### Data and code availability

- Analysis code is available at <https://doi.org/10.5281/zenodo.17453331>.
- Datasets and additional information required to reanalyze the data are available from the lead contact.

### ACKNOWLEDGMENTS

We thank Ilona Sauter for technical support. This work was supported by grants from the Deutsche Forschungsgemeinschaft to J.B. (FOR 5434); the European Research Council to J.B. (ERC AdG 883098 SleepBalance); the German Federal Ministry of Education and Research (BMBF) to the German Center for Diabetes Research (DZD e.V.); and the Hertie Foundation, Network for Excellence in Clinical Neuroscience, to N.N.

### AUTHOR CONTRIBUTIONS

Conceptualization, N.N. and J.B.; data collection, L.W. and N.N.; analysis, K.R. and N.N.; visualization, K.R. and N.N.; funding acquisition, N.N. and J.B.; supervision, N.N.; writing – original draft, K.R. and N.N.; revision of the manuscript, J.B. and N.N.

### DECLARATION OF INTERESTS

The authors declare no competing interests.

### DECLARATION OF GENERATIVE AI AND AI-ASSISTED TECHNOLOGIES IN THE WRITING PROCESS

ChatGPT was used to check grammar and spelling. After using this tool, the authors reviewed and edited the content as needed. No generative AI tools have been used to produce any new content.

### STAR★METHODS

Detailed methods are provided in the online version of this paper and include the following:

- **KEY RESOURCES TABLE**
- **EXPERIMENTAL MODEL AND STUDY PARTICIPANT DETAILS**
- **METHOD DETAILS**
  - Surgery
  - Head fixation procedure and sleep recordings
- **QUANTIFICATION AND STATISTICAL ANALYSIS**
  - EEG analyses - Detection of sleep SOs and spindles, calculation of power spectra
  - Two-photon imaging and analyses
  - Statistical analyses

### SUPPLEMENTAL INFORMATION

Supplemental information can be found online at <https://doi.org/10.1016/j.celrep.2025.116669>.

Received: February 21, 2025  
Revised: September 5, 2025  
Accepted: November 14, 2025

## REFERENCES

- Tononi, G., and Cirelli, C. (2014). Sleep and the price of plasticity: from synaptic and cellular homeostasis to memory consolidation and integration. *Neuron* 81, 12–34. <https://doi.org/10.1016/j.neuron.2013.12.025>.
- Rasch, B., and Born, J. (2013). About Sleep's Role in Memory. *Physiol. Rev.* 93, 681–766. <https://doi.org/10.1152/physrev.00032.2012>.
- Brodt, S., Inostroza, M., Niethard, N., and Born, J. (2023). Sleep-A brain-state serving systems memory consolidation. *Neuron* 111, 1050–1075. <https://doi.org/10.1016/j.neuron.2023.03.005>.
- Adamantidis, A.R., Gutierrez Herrera, C., and Gent, T.C. (2019). Oscillating circuitries in the sleeping brain. *Nat. Rev. Neurosci.* 20, 746–762. <https://doi.org/10.1038/s41583-019-0223-4>.
- Lecci, S., Fernandez, L.M.J., Weber, F.D., Cardis, R., Chatton, J.-Y., Born, J., and Lüthi, A. (2017). Coordinated infraslow neural and cardiac oscillations mark fragility and offline periods in mammalian sleep. *Sci. Adv.* 3, e1602026. <https://doi.org/10.1126/sciadv.1602026>.
- Steriade, M. (2006). Grouping of brain rhythms in corticothalamic systems. *Neuroscience* 137, 1087–1106. <https://doi.org/10.1016/j.neuroscience.2005.10.029>.
- Steriade, M., Nuñez, A., and Amzica, F. (1993). A novel slow (< 1 Hz) oscillation of neocortical neurons in vivo: depolarizing and hyperpolarizing components. *J. Neurosci.* 13, 3252–3265. <https://doi.org/10.1523/JNEUROSCI.13-08-03252.1993>.
- Rosanova, M., and Ulrich, D. (2005). Pattern-specific associative long-term potentiation induced by a sleep spindle-related spike train. *J. Neurosci.* 25, 9398–9405. <https://doi.org/10.1523/JNEUROSCI.2149-05.2005>.
- Klinzing, J.G., Niethard, N., and Born, J. (2019). Mechanisms of systems memory consolidation during sleep. *Nat. Neurosci.* 22, 1598–1610. <https://doi.org/10.1038/s41593-019-0467-3>.
- Fernandez, L.M.J., and Lüthi, A. (2020). Sleep Spindles: Mechanisms and Functions. *Physiol. Rev.* 100, 805–868. <https://doi.org/10.1152/physrev.00042.2018>.
- Latchoumane, C.-F.V., Ngo, H.-V.V., Born, J., and Shin, H.-S. (2017). Thalamic Spindles Promote Memory Formation during Sleep through Triple Phase-Locking of Cortical, Thalamic, and Hippocampal Rhythms. *Neuron* 95, 424–435.e6. <https://doi.org/10.1016/j.neuron.2017.06.025>.
- Niethard, N., Ngo, H.-V.V., Ehrlich, I., and Born, J. (2018). Cortical circuit activity underlying sleep slow oscillations and spindles. *Proc. Natl. Acad. Sci. USA* 115, E9220–E9229. <https://doi.org/10.1073/pnas.1805517115>.
- de Lima, A.D., and Morrison, J.H. (1989). Ultrastructural analysis of somatostatin-immunoreactive neurons and synapses in the temporal and occipital cortex of the macaque monkey. *J. Comp. Neurol.* 283, 212–227. <https://doi.org/10.1002/cne.902830205>.
- Packer, A.M., McConnell, D.J., Fino, E., and Yuste, R. (2013). Axo-Dendritic Overlap and Laminar Projection Can Explain Interneuron Connectivity to Pyramidal Cells. *Cereb. Cortex* 23, 2790–2802.
- Sejnowski, T.J., and Destexhe, A. (2000). Why do we sleep? *Brain Res.* 886, 208–223.
- Apicella, A.J., and Marchionni, I. (2022). VIP-Expressing GABAergic Neurons: Disinhibitory vs. Inhibitory Motif and Its Role in Communication Across Neocortical Areas. *Front. Cell. Neurosci.* 16, 811484. <https://doi.org/10.3389/fncel.2022.811484>.
- Sohn, J., Okamoto, S., Kataoka, N., Kaneko, T., Nakamura, K., and Hioki, H. (2016). Differential Inputs to the Perisomatic and Distal-Dendritic Compartments of VIP-Positive Neurons in Layer 2/3 of the Mouse Barrel Cortex. *Front. Neuroanat* 10, 124.
- Walker, F., Möck, M., Feyerabend, M., Guy, J., Wagener, R.J., Schubert, D., Staiger, J.F., and Witte, M. (2016). Parvalbumin- and vasoactive intestinal polypeptide-expressing neocortical interneurons impose differential inhibition on Martinotti cells. *Nat. Commun.* 7, 13664. <https://doi.org/10.1038/ncomms13664>.
- Brécier, A., Borel, M., Urbain, N., and Gentet, L.J. (2022). Vigilance and Behavioral State-Dependent Modulation of Cortical Neuronal Activity throughout the Sleep/Wake Cycle. *J. Neurosci.* 42, 4852–4866. <https://doi.org/10.1523/JNEUROSCI.1400-21.2022>.
- Aime, M., Calcini, N., Borsa, M., Campelo, T., Rusterholz, T., Sattin, A., Fellin, T., and Adamantidis, A. (2022). Paradoxical somatodendritic decoupling supports cortical plasticity during REM sleep. *Science* 376, 724–730. <https://doi.org/10.1126/science.abk2734>.
- Osorio-Forero, A., Cardis, R., Vantomme, G., Guillaume-Gentil, A., Katsioudi, G., Devenoges, C., Fernandez, L.M.J., and Lüthi, A. (2021). Noradrenergic circuit control of non-REM sleep substates. *Curr. Biol.* 31, 5009–5023.e7. <https://doi.org/10.1016/j.cub.2021.09.041>.
- Pi, H.-J., Hangya, B., Kvitsiani, D., Sanders, J.I., Huang, Z.J., and Kepecs, A. (2013). Cortical interneurons that specialize in disinhibitory control. *Nature* 503, 521–524. <https://doi.org/10.1038/nature12676>.
- Kullander, K., and Topolnik, L. (2021). Cortical disinhibitory circuits: cell types, connectivity and function. *Trends Neurosci.* 44, 643–657. <https://doi.org/10.1016/j.tins.2021.04.009>.
- Marshall, L., Helgadottir, H., Mölle, M., and Born, J. (2006). Boosting slow oscillations during sleep potentiates memory. *Nature* 444, 610–613. <https://doi.org/10.1038/nature05278>.
- Williams, L.E., and Holtmaat, A. (2019). Higher-Order Thalamocortical Inputs Gate Synaptic Long-Term Potentiation via Disinhibition. *Neuron* 101, 91–102.e4. <https://doi.org/10.1016/j.neuron.2018.10.049>.
- Adler, A., Zhao, R., Shin, M.E., Yasuda, R., and Gan, W.-B. (2019). Somatostatin-Expressing Interneurons Enable and Maintain Learning-Dependent Sequential Activation of Pyramidal Neurons. *Neuron* 102, 202–216.e7. <https://doi.org/10.1016/j.neuron.2019.01.036>.
- Neske, G.T., and Connors, B.W. (2016). Distinct Roles of SOM and VIP Interneurons during Cortical Up States. *Front. Neural Circuits* 10, 52. <https://doi.org/10.3389/fncir.2016.00052>.
- Aladjalova, N.A. (1957). Infra-Slow Rhythmic Oscillations of The Steady Potential of the Cerebral Cortex. *Nature* 179, 957–959. <https://doi.org/10.1038/179957a0>.
- Leopold, D.A., Murayama, Y., and Logothetis, N.K. (2003). Very Slow Activity Fluctuations in Monkey Visual Cortex: Implications for Functional Brain Imaging. *Cereb. Cortex* 13, 422–433. <https://doi.org/10.1093/cercor/13.4.422>.
- Lüthi, A., and Nedergaard, M. (2025). Anything but small: Microarousals stand at the crossroad between noradrenaline signaling and key sleep functions. *Neuron* 113, 509. <https://doi.org/10.1016/j.neuron.2024.12.009>.
- Hughes, S.W., Lorincz, M.L., Parri, H.R., and Crunelli, V. (2011). Infraslow (<0.1 Hz) oscillations in thalamic relay nuclei basic mechanisms and significance to health and disease states. *Prog. Brain Res.* 193, 145–162. <https://doi.org/10.1016/B978-0-444-53839-0.00010-7>.
- Zhang, Y., Karadas, M., Liu, J., Gu, X., Vöröslakos, M., Li, Y., Tsien, R.W., and Buzsáki, G. (2024). Interaction of acetylcholine and oxytocin neuromodulation in the hippocampus. *Neuron* 112, 1862–1875.e5. <https://doi.org/10.1016/j.neuron.2024.02.021>.
- Turi, G.F., Teng, S., Chen, X., Lim, E.C.Y., Dias, C., Hu, R., Wang, R., Zhen, F., and Peng, Y. (2025). Serotonin modulates infraslow oscillation in the dentate gyrus during non-REM sleep. *eLife* 13, RP100196. <https://doi.org/10.7554/eLife.100196>.
- Férezou, I., Cauli, B., Hill, E.L., Rossier, J., Hamel, E., and Lambolez, B. (2002). 5-HT<sub>3</sub> receptors mediate serotonergic fast synaptic excitation of

- neocortical vasoactive intestinal peptide/cholecystokinin interneurons. *J. Neurosci.* 22, 7389–7397.
35. Bell, L.A., Bell, K.A., and McQuiston, A.R. (2015). Activation of muscarinic receptors by ACh release in hippocampal CA1 depolarizes VIP but has varying effects on parvalbumin-expressing basket cells. *J. Physiol.* 593, 197–215. <https://doi.org/10.1113/jphysiol.2014.277814>.
36. Paspalas, C.D., and Papadopoulos, G.C. (1998). Ultrastructural evidence for combined action of noradrenaline and vasoactive intestinal polypeptide upon neurons, astrocytes, and blood vessels of the rat cerebral cortex. *Brain Res. Bull.* 45, 247–259. [https://doi.org/10.1016/s0361-9230\(97\)00327-4](https://doi.org/10.1016/s0361-9230(97)00327-4).
37. Toussay, X., Basu, K., Lacoste, B., and Hamel, E. (2013). Locus Coeruleus Stimulation Recruits a Broad Cortical Neuronal Network and Increases Cortical Perfusion. *J. Neurosci.* 33, 3390–3401. <https://doi.org/10.1523/JNEUROSCI.3346-12.2013>.
38. Jacobs, B.L., and Fornal, C.A. (1991). Activity of brain serotonergic neurons in the behaving animal. *Pharmacol. Rev.* 43, 563–578. [https://doi.org/10.1016/S0031-6997\(25\)06675-X](https://doi.org/10.1016/S0031-6997(25)06675-X).
39. McGinty, D.J., and Harper, R.M. (1976). Dorsal raphe neurons: depression of firing during sleep in cats. *Brain Res.* 101, 569–575. [https://doi.org/10.1016/0006-8993\(76\)90480-7](https://doi.org/10.1016/0006-8993(76)90480-7).
40. Lee, S.-H., and Dan, Y. (2012). Neuromodulation of brain states. *Neuron* 76, 209–222. <https://doi.org/10.1016/j.neuron.2012.09.012>.
41. Ferron, A., Siggins, G.R., and Bloom, F.E. (1985). Vasoactive intestinal polypeptide acts synergistically with norepinephrine to depress spontaneous discharge rate in cerebral cortical neurons. *Proc. Natl. Acad. Sci. USA* 82, 8810–8812. <https://doi.org/10.1073/pnas.82.24.8810>.
42. Ngo, H.-V.V., Martinetz, T., Born, J., and Mölle, M. (2013). Auditory closed-loop stimulation of the sleep slow oscillation enhances memory. *Neuron* 78, 545–553. <https://doi.org/10.1016/j.neuron.2013.03.006>.
43. Chang, H., Tang, W., Wulf, A.M., Nyasulu, T., Wolf, M.E., Fernandez-Ruiz, A., and Oliva, A. (2025). Sleep microstructure organizes memory replay. *Nature* 637, 1161–1169. <https://doi.org/10.1038/s41586-024-08340-w>.
44. Niethard, N., Hasegawa, M., Itokazu, T., Oyanedel, C.N., Born, J., and Sato, T.R. (2016). Sleep-Stage-Specific Regulation of Cortical Excitation and Inhibition. *Curr. Biol.* 26, 2739–2749. <https://doi.org/10.1016/j.cub.2016.08.035>.
45. Niethard, N., Brodt, S., and Born, J. (2021). Cell-Type-Specific Dynamics of Calcium Activity in Cortical Circuits over the Course of Slow-Wave Sleep and Rapid Eye Movement Sleep. *J. Neurosci.* 41, 4212–4222. <https://doi.org/10.1523/JNEUROSCI.1957-20.2021>.
46. Mölle, M., Marshall, L., Gais, S., and Born, J. (2002). Grouping of spindle activity during slow oscillations in human non-rapid eye movement sleep. *J. Neurosci.* 22, 10941–10947. <https://doi.org/10.1523/JNEUROSCI.22-24-10941.2002>.
47. Pologruto, T.A., Sabatini, B.L., and Svoboda, K. (2003). ScanImage: flexible software for operating laser scanning microscopes. *Biomed. Eng. Online* 2, 13. <https://doi.org/10.1186/1475-925X-2-13>.
48. Hattori, R., and Komiyama, T. (2022). PatchWarp: Corrections of non-uniform image distortions in two-photon calcium imaging data by patchwork affine transformations. *Cell Rep. Methods* 2, 100205. <https://doi.org/10.1016/j.crmeth.2022.100205>.
49. Keemink, S.W., Lowe, S.C., Pakan, J.M.P., Dylida, E., van Rossum, M.C.W., and Rochefort, N.L. (2018). FISSA: A neuropil decontamination toolbox for calcium imaging signals. *Sci. Rep.* 8, 3493. <https://doi.org/10.1038/s41598-018-21640-2>.
50. Grosmark, A.D., Mizuseki, K., Pastalkova, E., Diba, K., and Buzsáki, G. (2012). REM sleep reorganizes hippocampal excitability. *Neuron* 75, 1001–1007. <https://doi.org/10.1016/j.neuron.2012.08.015>.
51. Wilcox, R.R. (1994). The Percentage Bend Correlation Coefficient. *Psychometrika* 59, 601–616. <https://doi.org/10.1007/BF02294395>.
52. Pernet, C.R., Wilcox, R., and Rousselet, G.A. (2012). Robust correlation analyses: false positive and power validation using a new open source matlab toolbox. *Front. Psychol.* 3, 606. <https://doi.org/10.3389/fpsyg.2012.00606>.



## STAR★METHODS

### KEY RESOURCES TABLE

REAGENT or RESOURCE	SOURCE	IDENTIFIER
<b>Bacterial and virus strains</b>		
AAV9-GCaMP8m	Addgene, USA	RRID: Addgene_162375
AAV9-Flex-CAG-tdTomato	Addgene, USA	RRID: Addgene_28306
<b>Experimental models: Organisms/strains</b>		
VIP-cre (B6J.Cg-Vip <sup>tm1(cre)</sup> Zjh/ArcKJ)	The Jackson Laboratory	RRID: IMSR_JAX:031628
PV-Cre (B6;129P2-Pvalb <sup>tm1(cre)</sup> Arbr/J)	The Jackson Laboratory	RRID: IMSR_JAX:008069
SOM-Cre (Sst <sup>tm2.1(cre)</sup> Zjh/J)	The Jackson Laboratory	RRID: IMSR_JAX:013044
<b>Software and algorithms</b>		
CED Spike2	Cambridge Electronic Design, UK	RRID: SCR_000903
ScanImage	MBF Bioscience, LLC	RRID: SCR_014307
MATLAB	MathWorks, Inc.	RRID: SCR_001622
Patchwarp toolbox	Ryoma Hattori	DOI: <a href="https://doi.org/10.5281/zenodo.8368714">https://doi.org/10.5281/zenodo.8368714</a>
FISSA	Rochefort Lab	DOI: <a href="https://doi.org/10.1038/s41598-018-21640-2">https://doi.org/10.1038/s41598-018-21640-2</a>
Python Programming Language	Python Software Foundation	RRID: SCR_008394

### EXPERIMENTAL MODEL AND STUDY PARTICIPANT DETAILS

For the experiments, healthy adult male VIP-cre (B6J.Cg-Vip<sup>tm1(cre)</sup>Zjh/ArcKJ) mice (RRID: IMSR\_JAX:031628;  $n = 9$ ), PV-Cre (B6;129P2-Pvalb<sup>tm1(cre)</sup>Arbr/J) mice (RRID:IMSR\_JAX:008069;  $n = 4$ ) and SOM-Cre (Sst<sup>tm2.1(cre)</sup>Zjh/J) mice (RRID: IMSR\_JAX:013044;  $n = 4$ ) were used. Data from PV- and SST-cre animals were taken from previously published work<sup>44</sup> and reanalyzed for infraslow dynamics. At the time of data collection all animals were not involved in previous experiments. The mice were housed in groups of up to five animals under temperature-controlled and humidity-controlled conditions ( $22 \pm 2^\circ\text{C}$ ; 45–65%) and a 12/12 h light/dark cycle. All recordings started during the first hour of the light phase, and only male mice older than twelve weeks were recorded. General procedures were the same as described previously.<sup>45</sup> All experiments were approved by the local institutions in charge of animal welfare (Regierungspräsidium Tübingen, State of Baden-Wuerttemberg, Germany).

### METHOD DETAILS

#### Surgery

Animals were anesthetized using a three-component anesthesia (0.05 mg Fentanyl, 5.00 mg Midazolam, and 0.5 mg Medetomidin per 1 kg body weight), supplemented with isoflurane. Afterward, the animals were mounted on a stereotaxic frame, and body temperature was continuously monitored and maintained at  $37^\circ\text{C}$ . A custom-made headpost was glued to the skull and cemented with dental acrylic (Palapress; Kulzer, Germany).

Virus injection and the implantation of the imaging window followed headpost implantation. To this end, a craniotomy was made above the sensorimotor cortex (+1.1 mm caudal and 1–1.3 mm lateral from the bregma) with  $1.2 \times 2$  mm dimensions. Two viruses—AAV9-GCaMP8m ( $1.8 \times 10^{12}$  genomes/ml) and AAV9-Flex-CAG-tdTomato ( $5.6 \times 10^{11}$  genomes/ml) (Addgene, USA)—were injected at multiple sites within the craniotomy area (70 nL/site, 3–5 min per injection). The injections were made at depths ranging from 130 to 280  $\mu\text{m}$ . After the virus injections, a  $1 \times 1.5$  mm imaging window was implanted. The space between the skull and the imaging window was filled with 1.5–2% agarose, and the window was secured with dental acrylic. Frontal and parietal EEG electrodes (stainless steel wire, Science Products, Germany) were implanted on the cortical surface (frontal +1.2 mm anterior and +1.2 mm lateral; parietal –2.5 mm posterior and –2.5 mm lateral from bregma). Reference electrodes were placed on the brain surface 1 mm relative to  $\lambda$ . Additionally, two wire electrodes were inserted into the neck muscle for EMG recordings (Science Products). Following surgery, all animals were returned to their home cage and were single-housed for the rest of the experiments. They were given at least 10 days to recover before imaging sessions started.

### Head fixation procedure and sleep recordings

After one week of daily handling sessions (10 min per day), the animals were habituated to head fixation. The habituation protocol consisted of four daily sessions over one week, with progressively increasing fixation durations of 30 s, 3 min, 10 min, and 30 min. Each session was interspersed with 10-min rest intervals. Habituation was completed at least 24 h before the first imaging session, which was conducted during the animals' rest phase, between 7:00 a.m. and 7:00 p.m.

Sleep stages were identified during the imaging sessions based on EEG and EMG recordings. The EEG and EMG signals were amplified, filtered (EEG: 0.01–300 Hz; EMG: 30–300 Hz), and sampled at a rate of 32 kHz using a Digital Lynx SX amplifier (Neuralynx, USA). The brain state of the mouse was classified as Wake, SWS, or REM sleep in 10-s epochs based on EEG and EMG signals. The classification was performed using custom scripts written in CED Spike2 (Cambridge Electronic Design, UK).

## QUANTIFICATION AND STATISTICAL ANALYSIS

### EEG analyses - Detection of sleep SOs and spindles, calculation of power spectra

For detecting discrete SO and spindle events during SWS, algorithms were adopted from previous studies.<sup>12,46</sup> In brief, for detecting SOs, the EEG was bandpass filtered between 0.1 and 4 Hz (3<sup>rd</sup> order Butterworth filter). Then, all positive-to-negative zero crossings of the signal and the local minimum and maximum between each two successive crossings were marked. Intervals between two succeeding positive-to-negative zero-crossings were identified as an SO event if the length of this interval was between 0.4 and 2 s and if the minimum amplitude and minimum-to-maximum amplitude were >66.6% of the average of the respective amplitude values across the whole recording. The enclosing zero-crossings represent the onset and end of the corresponding SO cycle for these remaining events.

To detect spindles, the EEG signal was band-pass filtered between 11 and 16 Hz (3<sup>rd</sup> order Butterworth filter). The envelope of the filtered signal was extracted using the absolute value of the Hilbert transform. A spindle event was defined as occurring when the envelope exceeded 1.5 standard deviations (SD) for at least 0.5 s. Within this time window, the envelope was required to reach 2 SD for a minimum of 0.25 s and exceed 2.5 SD at least once. The onset and end of a spindle event were marked by the positive and subsequent negative crossings of the 1.5 SD threshold, respectively. Events lasting longer than 2.5 s were excluded from the analysis.

### Two-photon imaging and analyses

*In vivo* imaging was performed using a two-photon microscope based on the MOM system (Sutter, USA) controlled by ScanImage software.<sup>47</sup> The light source was a pulsed Ti:sapphire laser ( $\lambda = 940$  nm; Chameleon; Coherent, USA). Red and green fluorescence photons were collected with a 20 $\times$  water immersion objective lens (Zeiss, Germany), separated by a 565 nm dichroic mirror (565dxcx, Chroma, USA) and barrier filters (green: ET525/70 m-2p; red: ET605/70 m-2p), and measured using photomultiplier tubes (H10770PA-40, Hamamatsu Photonics, Japan). Imaging frames were visually inspected to minimize cross-talk between green and red channels. The imaging frames consisted of 256  $\times$  256 pixels, and the frame rate was 4.25 Hz (235 ms per frame). All Images were recorded in layers 2 and 3 at a depth of 150–250  $\mu$ m.

The lateral motion was corrected using MATLAB (R2020b; MathWorks, USA) with the Patchwarp toolbox (1.3.2).<sup>48</sup> Regions of interest (ROIs) containing individual neurons were drawn manually and later neuropil-corrected and extracted using FISSA (1.0.0)<sup>49</sup> in a separate Anaconda environment with Python (3.11.5). Next, we removed the time frames previously tagged because of immersion medium disturbances. VIP-INs were manually detected by the red fluorescence signal expressed by AAV9-Flex-CAG-tdTomato. The cell traces were transformed into percent signal change, where the baseline for each cell was defined as the 20th percentile value of all frames within a symmetric moving window with a width of 1530 frames (6 min). We added a constant of 1 equivalent to 100% to the resulting values and divided the baseline-corrected  $\text{Ca}^{2+}$  traces by these quantile values to generate  $\Delta F/F$  traces.

### Statistical analyses

All sleep-stage referring analysis investigates differences within epochs of a specific brain state (Wake, SWS, REM epochs) or between epochs. Based on previous work that characterized changes in hippocampal activity across entire Wake, SWS, and REM sleep episodes,<sup>50</sup> we divided each epoch of SWS, REM sleep, and wakefulness with minimum durations of 50 s into thirds and calculated active frame proportions for each cell during the 1<sup>st</sup>, 2<sup>nd</sup>, and 3<sup>rd</sup> third of each epoch. Calcium activity was then performed using a mixed ANOVA on the active frames of each cell, with the group factors "VIP/nonVIP" representing the different kinds of cells, and a "Stage" factor representing the three different stages Wake, SWS, REM sleep and their interaction with the random effect grouping variable "Cell" (a unique identifier for each cell). Similar ANOVAs were used to analyze within-epoch changes (3<sup>rd</sup>-1<sup>st</sup> third) in calcium activity. For correlation analyses of within-epoch changes, Percentage Bend correlation coefficients<sup>51</sup> were calculated because of their robustness against univariate outliers and violations of normality.<sup>52</sup>

To analyze calcium activity during SO, spindle, and SO-spindle events, the median cell population (VIP/nVIP) fluorescence was extracted relative to a Baseline phase prior to the event. Here, ANOVAs included a repeated measures Phase factor representing the Downstate, Upstate, and After phases for SO-related analyses and for spindle-related analyses, the During and After phases. For SOs, the baseline was defined as the 0.75-s interval before the first zero crossing of the SO. The Downstate phase was represented by the 235-ms interval (=1 frame) around the downstate peak. The Upstate phase began at the negative to positive zero

crossing following the negative peak and lasted until the next positive to negative zero crossing. The After phase represented the following 0.75-s interval. For spindle-related analyses, the baseline was defined by the 0.75-s interval preceding spindle onset. The During phase lasted from spindle onset to the end of the spindle, and the After phase by the 0.75-s interval starting with the end of the spindle.

Infraslow oscillations in VIP and nonVIP, as well as PV and SST cell  $\text{Ca}^{2+}$  activity and EEG sigma and SWA power were analyzed using MATLAB R2023a (MathWorks, USA) autocorrelation functions (ACFs) and cross-correlation functions (CCFs). ACFs and CCFs were performed using a bin size of 235 ms on the median  $\Delta F/F$  signal and the respective EEG power signals after filtering these signals using a 0.01–0.1 Hz 3<sup>rd</sup> order Butterworth filter. ACFs and CCFs were calculated separately for individual SWS and REM sleep epochs that had a minimum duration of 120 s and 50 s, respectively. The resulting correlation coefficients were Fisher z-transformed, and tests of mean coefficients against zero, as well as between conditions (VIP vs. nonVIP, SWS vs. REM), were performed using t-tests. The resulting *p*-values were adjusted for multiple comparisons using the Bonferroni-Holm method. Amplitudes of infraslow rhythms identified through ACFs were estimated by calculating the absolute values of the Hilbert transformed values after filtering the mean  $\Delta F/F$  signal of the VIP population from 0.01 to 0.03 Hz using a 6<sup>th</sup> order Butterworth filter. Amplitude values were compared between states using a Welch separate variances *t* test to compensate for unequal variances.

Temporal relationships between  $\text{Ca}^{2+}$  activity of VIP cells and SOs and spindles were additionally assessed using event-correlation histograms covering a  $\pm 50$  s interval around the negative halfwave peak of SOs and spindle onsets, respectively. Mean  $\text{Ca}^{2+}$  activity in specific time intervals before and after the target events was assessed using ANOVA, including a repeated measure before/after and a VIP/nonVIP group factor. To determine the fraction of interneurons that are anti-correlated with infraslow sigma band power, we calculated the difference between  $\Delta F/F$  signals during the positive and negative half waves of the infraslow sigma oscillation for wake, SWS, and REM sleep separately for each cell.

**Cell Reports, Volume 44**

**Supplemental information**

**VIP interneuron activity during sleep  
conveys the cortical infraslow oscillation**

**Kilian Rolle, Louisa Weber, Jan Born, and Niels Niethard**



**Table S1. Cell and epoch contributions of animals, related to all Figures.**

Animal	Sessions	# Cells		Duration (in min)		
		VIP	nonVIP	WAKE	SWS	REM
1	4	25	275	301.19	201.00	15.51
2	4	25	262	374.84	281.38	43.53
3	3	20	134	120.71	138.67	24.17
4	5	28	332	271.20	278.06	60.51
5	2	11	81	315.20	110.20	16.34
6	1	7	42	137.84	67.36	1.83
7	1	3	33	114.51	38.02	0.00
8	5	21	183	701.39	333.12	15.17
9	1	2	14	115.67	97.56	2.67
<b>Sum</b>	<b>26</b>	<b>142</b>	<b>1356</b>	<b>2452.55</b>	<b>1545.37</b>	<b>179.73</b>
<b>Mean</b>	<b>2.89</b>	<b>15.78</b>	<b>150.67</b>	<b>272.51</b>	<b>171.71</b>	<b>19.97</b>
<b>±SEM</b>	<b>0.56</b>	<b>3.37</b>	<b>39.31</b>	<b>63.22</b>	<b>35.23</b>	<b>6.77</b>

Contribution of the individual animals to the data set. From left to right: Animal: indicates subject #, number of recording Sessions for each animal, number of recorded VIP and nonVIP cells (# Cells) across all sessions, time (Duration) spent in Wake, SWS, and REM sleep across all sessions. Bottom lines indicate sums across all animals and means ( $\pm$ SEM) for the sample. This table is related to all analysis.

**Table S2. Slow wave sleep related events, contribution of animals related to the analysis of slow wave sleep specific events, related to Figures 3 and 7.**

Animal	Events		
	SO-spindle	SO	Spindle
1	242	2125	359
2	431	3150	583
3	237	1365	315
4	386	2757	477
5	123	1173	150
6	74	578	95
7	37	410	22
8	614	3324	393
9	144	1010	118
<b>Sum</b>	2288	15892	2512
<b>Mean</b>	254.22	1765.78	279.11
<b>±SEM</b>	63.19	368.70	63.99

Number of solitary SOs, solitary spindles, and SO-spindle events identified in each animal.

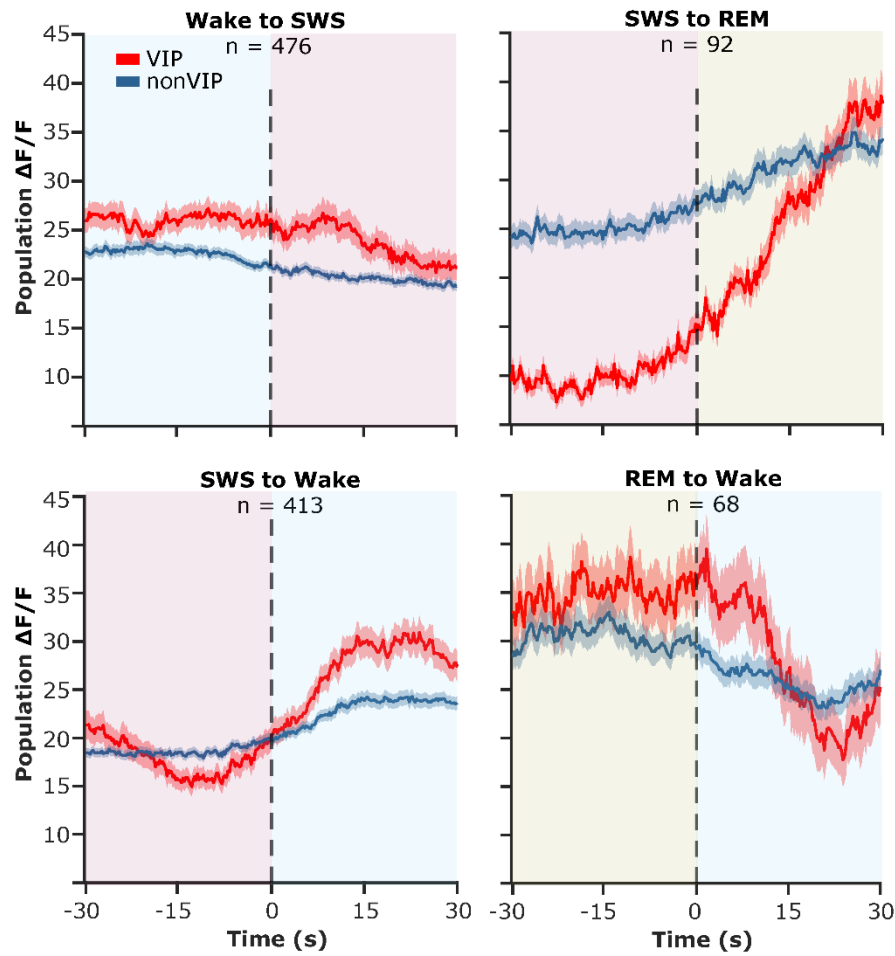


**Figure S1,  $\Delta F/F$  signal of VIP and nonVIP cells at sleep stage transitions, related to Figure 1.** Mean  $\pm$  SEM  $\Delta F/F$  signals of VIP (red) and nonVIP (blue) cells time-locked to the sleep stage transitions (indicated above). The dashed line indicates the time of the stage transition.

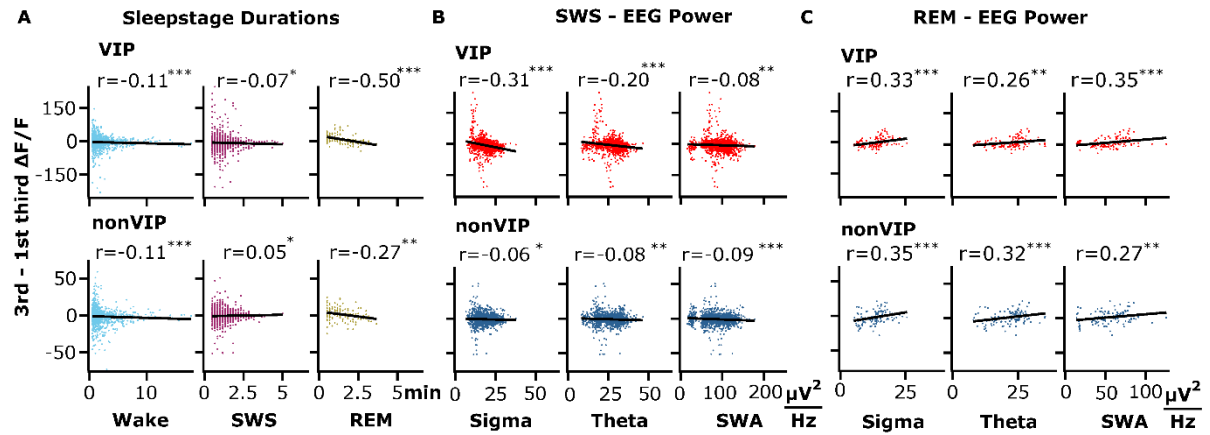


**Figure S2. Relationship of within-epoch change in VIP and nonVIP cell activity with the duration and EEG characteristics of the epoch, related to Figure 2.** Scatterplots illustrating for VIP cells (top) and nonVIP cells (bottom) correlations between the within-epoch change in  $\text{Ca}^{2+}$  activity (3rd - 1st third of respective epoch) and **A)** the duration of the respective (from left to right) Wake, SWS, and REM sleep epochs, **B)** the mean power in the 0.5-4 Hz SWA, 4-9 Hz theta, and 11-16 Hz sigma EEG frequency bands during SWS epochs, as well as **C)** during REM sleep epochs. Percentage bend coefficients and their significance are indicated. \* $p < 0.05$ , \*\* $p < 0.01$ , \*\*\* $p < 0.001$ .



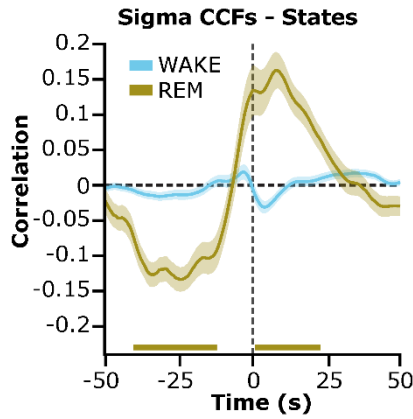


**Figure S3, the coupling between the ~0.02 Hz infraslow oscillation in VIP cell activity and EEG sigma is most distinct during slow wave sleep, related to Figures 4 and 6.** Mean ( $\pm$ SEM) cross-correlation functions (CCFs) between 11-16 Hz EEG sigma and VIP cell  $\text{Ca}^{2+}$  activity during  $n = 886$  Wake epochs (blue) and during  $n = 81$  REM sleep epochs (gold, all epochs  $\geq 50$  s duration). Coloured horizontal bars at the bottom indicate the significance of respective correlation coefficients ( $p < 0.05$ , after Bonferroni-Holm correction). Note that only the CCF for REM sleep reveals significant minima and maxima, which, however, extend over broad time ranges, speaking against a specifically timed relationship between the respective parameters.